STRUCTURE CHANGES DURING PSEUDOELASTIC DEFORMATION OF CuAlMn SINGLE CRYSTALS

J. DUTKIEWICZ[1], H. KATO[2], S. MIURA[2], U. MESSERSCHMIDT[3] and M. BARTSCH[3]

[1]Institute of Metallurgy and Materials Science of the Polish Academy of Sciences, 30-059 Kraków ul. Reymonta 25, Poland, [2]Department of Engineering Physics and Mechanics, Faculty of Engineering, Kyoto University, Kyoto 606-01, Japan and [3]Max-Planck Institute of Microstructure Physics, Weinberg 2, Halle/Saale, D-06120 Germany

Abstract—Structure changes during pseudoelastic deformation of CuAlMn single crystals were investigated using *in situ* optical and high-voltage electron microscopy (HVEM). Several crystal orientations were investigated, from an irrational to $\langle 100 \rangle$ and $\langle 110 \rangle$ tensile axis and plane orientations in the case of thin foils. The composition of the alloy was chosen such as to obtain superelastic behavior at room temperature. Optical microstructures allowed to identify parallel plates at the beginning of the stress plateau, the number of which increased with strain. The stress/temperature phase diagram was established within the range of existence of γ_1' and β_1'. During *in situ* HVEM deformation in the $\langle 100 \rangle$ direction of γ_1' plates nucleated on pre-existing ones. At later deformation stages 18R martensite was formed in stacks of narrow needles. The following crystallographic relationship was observed: $[001]\beta_1\|[010]\beta_1'$, γ_1' and $[110]\beta_1\|[001]\beta_1'$, γ_1'. A small permanent deformation observed after stress release was connected with the presence of residual martensite of a high random stacking fault density and consisting often of α_1', γ_1' and β_1' martensite layers. During deformation in the $\langle 110 \rangle$ direction a larger permanent deformation and a density of dislocations was observed. *Copyright © 1996 Acta Metallurgica Inc.*

INTRODUCTION

In order to understand the mechanism of pseudoelastic deformation in β-phase copper base alloys, *in situ* optical microstructure observations during tensile deformation were reported on CuAlNi [1–5], CuZnSn [3, 6], CuAlZn [7–11] CuSn [12] and CuAlMn [13] alloys. They showed different results regarding the nucleation and growth of various kinds of stress-induced martensites, their orientation with respect to the tensile axis [1] and the interaction with grain boundaries during particular deformation stages. The formation of martensitic plates in single crystals occurs often in the form of parallel plates which grow during deformation, but interfaces do not disappear completely [2]. This is surprising since an increase of the number of interfaces increases the internal energy of the system [14] and one would expect a coalescence of the individual plates. On the other hand, at the resolution of the optical microscope one cannot distinguish narrow plates of a different orientation from interfaces within one plate. From a change of martensite morphology one can draw conclusions on the structure of martensite, but it has to be confirmed by X-ray diffraction. Simultaneous X-ray diffraction studies during pseudoelastic deformation of CuAlFe [14] alloys allowed to identify the following sequence of martensitic phases formation with increasing strain: $\gamma_1' \rightarrow \beta_1' \rightarrow \alpha_1'$. Additionally the crystallographic

relationships were found between the parent and the martensitic phase. *In situ* deformation during transmission electron microscope observation of CuAlZn and CuAlFe alloys [10, 15] yielded additional information regarding the defect and interface structure [10] as well as the crystal structure and orientation of particular plates forming at successive deformation stages [15]. This method was therefore chosen to study a development of martensitic structures in CuAlMn alloys, which has been shown to consist of γ_1', β_1' and α_1' phases [13].

EXPERIMENTAL PROCEDURE

Copper alloys containing 20.8 at.% Al and 9.5 at.% Mn were made by melting 4 N purity Cu and Al and 3 N purity Mn together in an induction furnace under argon atmosphere. Single crystals in the shape of rods of 8 mm diameter and 80 mm length were prepared using the Bridgman method. After annealing at 850°C and quenching in water of 55°C (to prevent the stabilization of quenched in martensite) specimens were cut out using a spark erosion machine. Characteristic transformation temperatures were determined using electrical resistivity measurements or a DuPont thermal analyser. Tensile tests of bulk samples at irrational (random) orientation (determined using the back Laue reflection method as [0.151, 0.200, 0.968]) were performed

using an Instron testing machine at a strain rate of 8.33×10^{-3}/s. Specimens for *in situ* straining experiments were cut out in the form of thin sheets of $0.2 \times 3 \times 8$ mm parallel to $\{001\}$ or $\{110\}$ β_1 planes and $\langle 100 \rangle$ or $\langle 110 \rangle$ tensile directions. Afterwards, a two-stage electrolytic polishing was applied; first using a platinum mask in CrO_3 saturated phosphoric acid to create a flat dimple in the center, then in 1/3 HNO_3 2/3 CH_3OH solution at $-30°C$ until perforation. *In situ* tensile experiments were performed using JEOL 1000 kV electron microscope equipped with a tensile stage designed by Messerschmidt and Appel [16]. It allowed simultaneous recording of TEM images using video equipment and load/elongation curves up to maximum elongation of 60 μm, which corresponds to *ca* 2% strain for the samples applied.

RESULTS AND DISCUSSION

Figure 1 shows an electrical resistivity curve of an as-quenched single crystal. Transformation temperatures were determined from the intersection of the tangent lines as marked in Fig. 1. All the characteristic transformation temperatures, including $M_s = 256$ K, $M_f = 241$ K, $A_s = 254$ K and $A_f = 268$ K are below room temperature. Similar data (with a slightly broader hysteresis) were obtained from microcalorimetric measurements at the cooling/heating rate of 10 K/min. Figure 2 shows stress/strain curves of a single crystal (of the orientation shown in the lower right corner) performed at various temperatures. Their change with temperature is similar to that reported for tensile tests in the $\langle 100 \rangle$ direction of CuAlNi [3, 5] and CuAlMn alloys [12]. The stress/strain curve below M_f
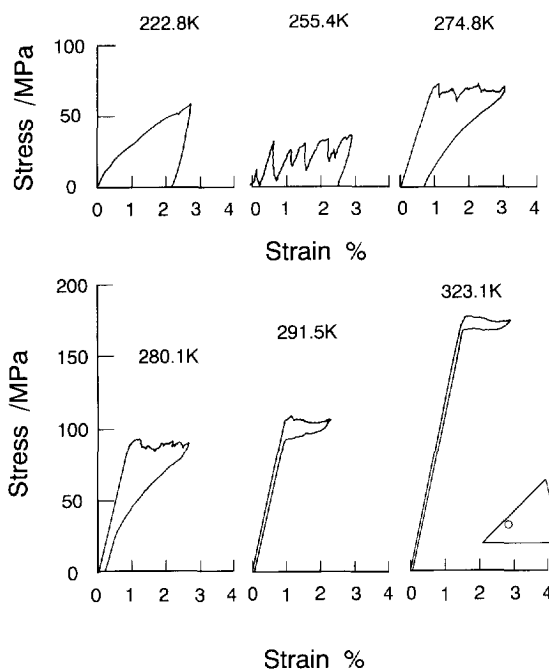
Fig. 2. Tensile stress/strain curves of the investigated CuAlMn alloy single crystal at various temperatures.

(222.8 K, Fig. 2), where a thermal martensite is deformed, is characterized by a smooth curve, since during the deformation only a movement of martensitic interfaces occurs. The residual strain left after unloading was completely recovered by heating the specimen above A_f. The stress/strain curve obtained very close to the M_s temperature (at 255.4 K) shows a large serration due to the formation of stress induced γ_1' (2H) martensite. The stress/strain curves above A_f show a pseudoelastic behavior, however the complete superelastic curve cannot be obtained between M_s and 290 K. In this temperature range the martensite induced during tensile deformation cannot completely return to the parent phase during unloading. The stress required for a shift of martensitic interfaces [Fig. 2(a)] is lower than that to form γ_1' martensite [Figs 2(c) and (d)], while a highest stress is necessary to form β_1' martensite [12].

In order to investigate the origin of differences in the stress/strain behavior, *in situ* optical microscope observations were carried out during tensile tests. Figure 3 shows a set of microstructures taken at various stages of pseudoelastic deformation at 299 K, as marked in the stress/strain curve. In (a) a few plates have formed at the initial stage of the stress plateau. With increasing strain new plates with flat interfaces form in front of the others. Their density increases and as the result the parent/martensite interface advances in the direction of the tensile axis (c). At (e), which corresponds to the highest stress value, the whole area is covered by the martensitic needles and boundaries between needles are barely seen. During unloading the reverse movement of
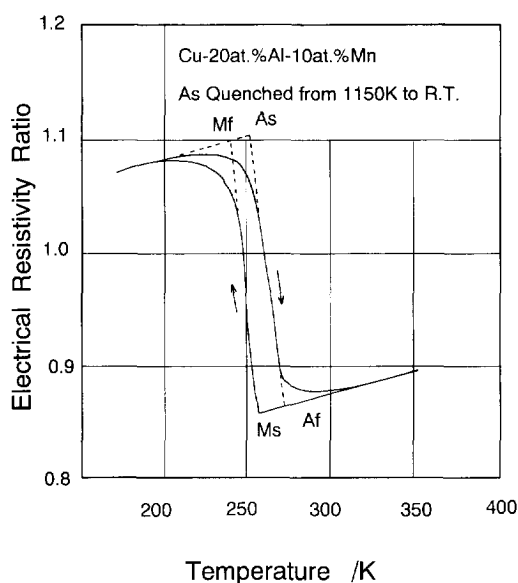

Fig. 1. Change of electrical resistivity vs temperature of the investigated CuAlMn alloy, allowing estimation of characteristic transformation temperatures.

interfaces and gradual disappearance of martensitic plates were observed [(E)–(H)]. The permanent deformation of *ca* 1% retained after strain release is most probably due to the deformation of the specimen near the grip. The large shear strain associated with a single interface transformation

generates inhomogeneous stress distribution and may cause a local plastic deformation of the specimen. *In situ* observation of the center of the specimen confirmed the lack of martensite after unloading.

The stress/strain curves of the deformation between M_s and 290 K were different from those
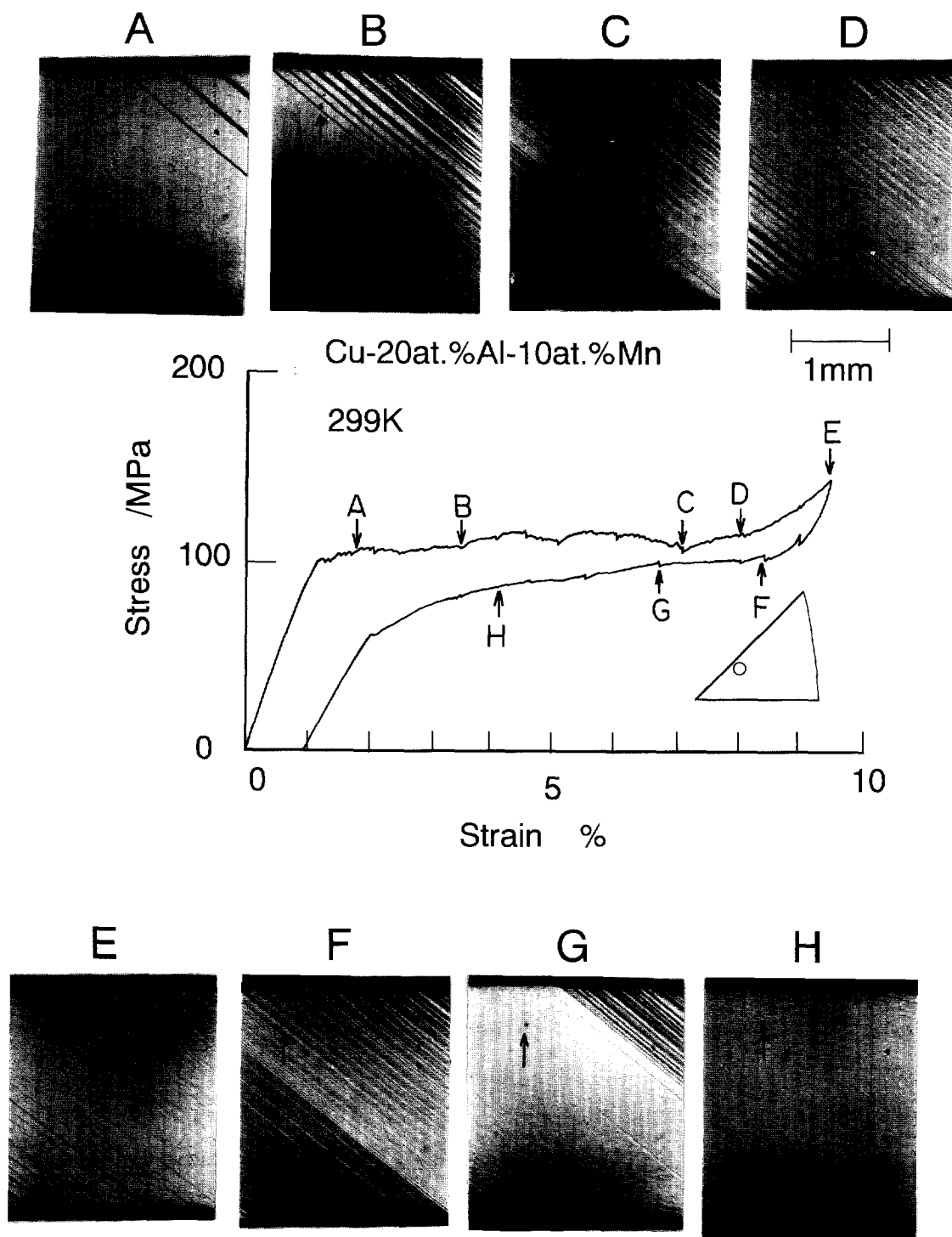
Fig. 3. *In situ* optical microscopy observation of the surface of the tensile tested specimen at various stages of pseudoelastic deformation at 299 K.

taken above 290 K. The flow stress yielding the stress-induced martensitic transformation shows large serration's visible in Fig. 4(a). The width of the serration becomes larger and the fraction of the strain recovery becomes smaller with decreasing deformation temperature. Microstructures taken *in situ* during the initial period of strain increase are given in Fig. 4(b). The plates are different from those in Fig. 3, being much thinner and often of irregular shape. The macroscopic parent/martensite interface is well defined. It shows similarities to γ_1' martensite in single crystals of CuAlMn alloys with different composition as described in [12]. The temperature dependence of the critical stress to induce martensite is plotted in Fig. 5. It follows a linear relationship as already reported for several copper alloys [1, 3, 12, 17, 18]. At the temperature just above M_s, the upper and lower yield stresses have been taken, which are indicated as σ_U and σ_L in Fig. 4(a). The upper yield points σ_U and generally the superelastic yield stresses can be approximated in the same manner as $\sigma = 2.20(T\text{-}238)$ (MPa). On the other hand, the lower yield points σ_L show another relationship represented as $\sigma = 2.64(T\text{-}253)$ (MPa) and the extrapolation of this line corresponds to M_s temperature. These results support the assumption that the crystal structure of the martensite formed at the higher stress range is β_1' and that of the lower stress range is γ_1'. During deformation just above M_s the β_1' martensite is induced at first, while the sudden relaxation of the flow stress corresponds to the formation of the γ_1' martensite. This situation is due to the fact that much lower stress is needed to form 2H martensite than 18R, as observed also in previous studies on CuAlNi [1], CuAlFe [14] and CuAlMn alloys [12].

Figure 6(a) shows a load/elongation curve taken from a single crystal in a $[001]\beta_1$ orientation tested in tension in a $[100]\beta_1$ direction. A series of micrographs was reproduced from video recordings taken during *in situ* HVEM deformation. The first micrograph of the series was taken just before attaining the yield stress [as marked in Fig. 6(a)], but already a large plate existed in the crystal [Fig. 6(b)]. The following micrograph [Fig. 6(c)] shows the nucleation of a small single needle at the existing one. It grows parallel to the tensile axis. The following micrographs show the formation of other needles near the first one [Figs 6(d) and (e)] and the nucleation of needles in transverse direction [Fig. 6(e)]. At a final stage small plates join into the single large plate. This observation is consistent with *in situ* optical microscope observations, where the nucleation of parallel plates was shown.

Figure 7(a) exhibits a tip of a γ_1' plate with a step-like martensite/parent interface. The diffraction pattern (b) of the β_1 parent phase shows cross-like side bands near the fundamental and superlattice reflections. Corresponding modulations perpendicular to the excited $\langle 100 \rangle$ row of reflections suggest the presence of $\langle 110 \rangle \{110\}$ static displacement waves, as pointed out for β-type copper base alloys [19, 20]. Their origin is not due to spinodal decomposition, since the modulation distance does not correspond to the wavelength of the modulations. Some influence of surface effects cannot be excluded, as already suggested in [20]. The contrast of the modulations does not depend on the applied stress. The selected area diffraction pattern [SADP, Fig. 7(c)] of the martensite exhibit 2H reflections at a [010] zone axis orientation. The following crystallographic relationship with the β_1 parent phase exists: $[001]\beta_1 \| [010]\gamma_1'$
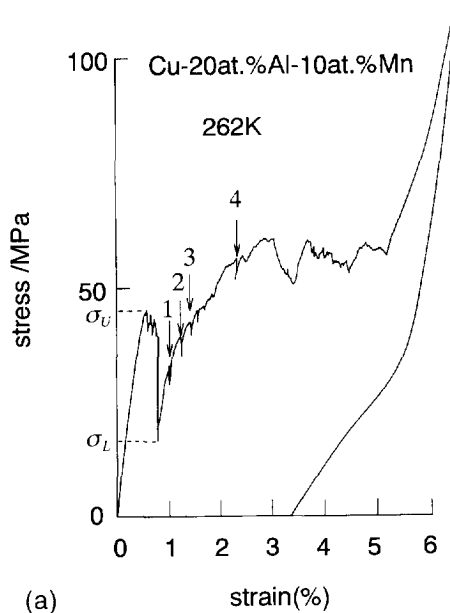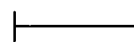

Fig. 4 (a). (*see caption opposite.*)

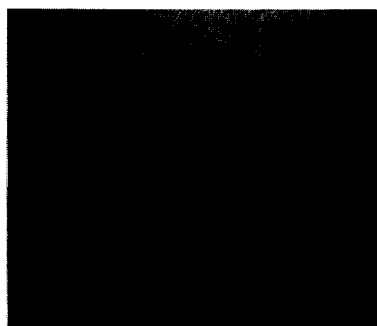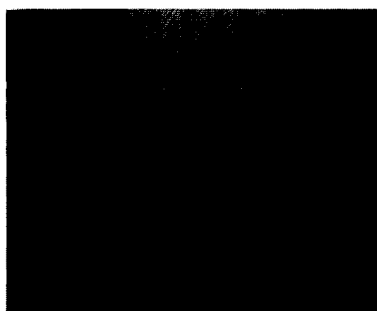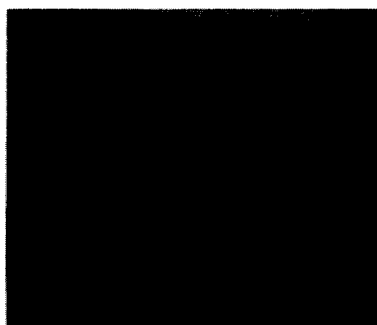Cu-20at.%Al-10at.%Mn

deformed at 262K 0.5mm

1) 1.0%

↓

2) 1.2%

↓

3) 1.4%

↓

4) 2.3%

(b)

Fig. 4. Stress/strain curve at 262 K, 6 K above M_s (a) and optical micrographs (b) taken at various stage of deformation in the parent state.
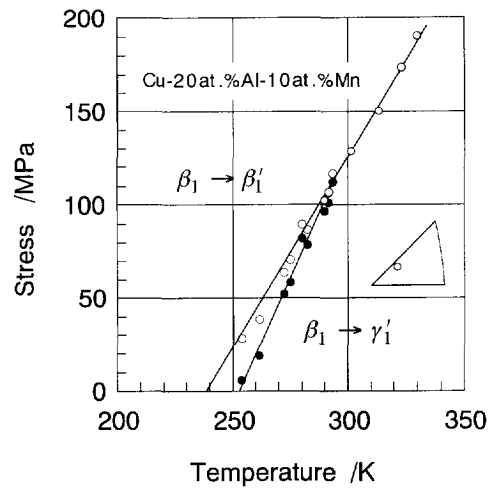
Fig. 5. Temperature dependence of the critical stress to induce two types of martensite.
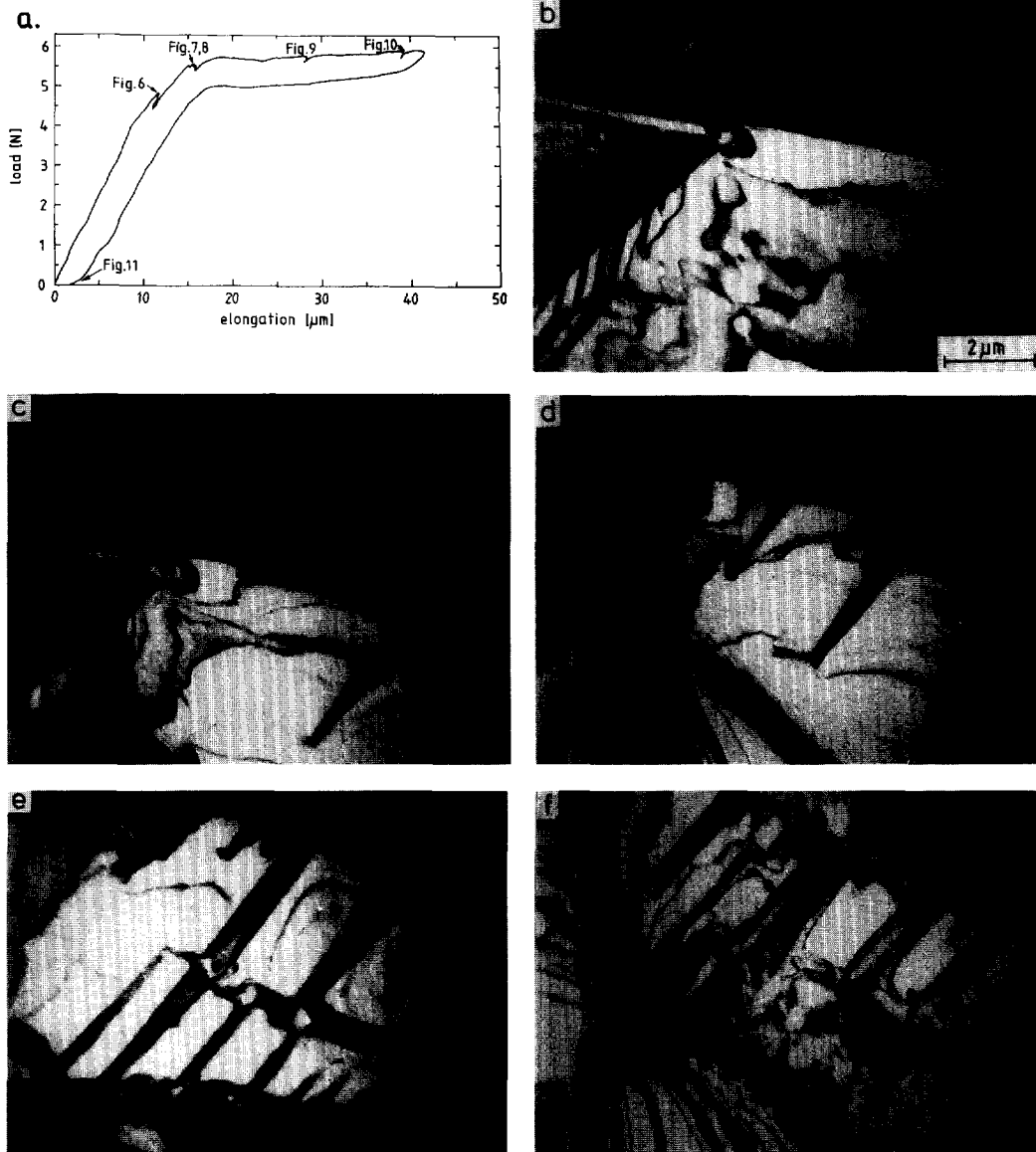

Fig. 6. (a) Load/elongation curve recorded during *in situ* HVEM deformation in the $\langle 100 \rangle \beta_1$ direction.
(b)–(f) Set of transmission electron micrographs recorded during *in situ* tensile deformation. Points in the
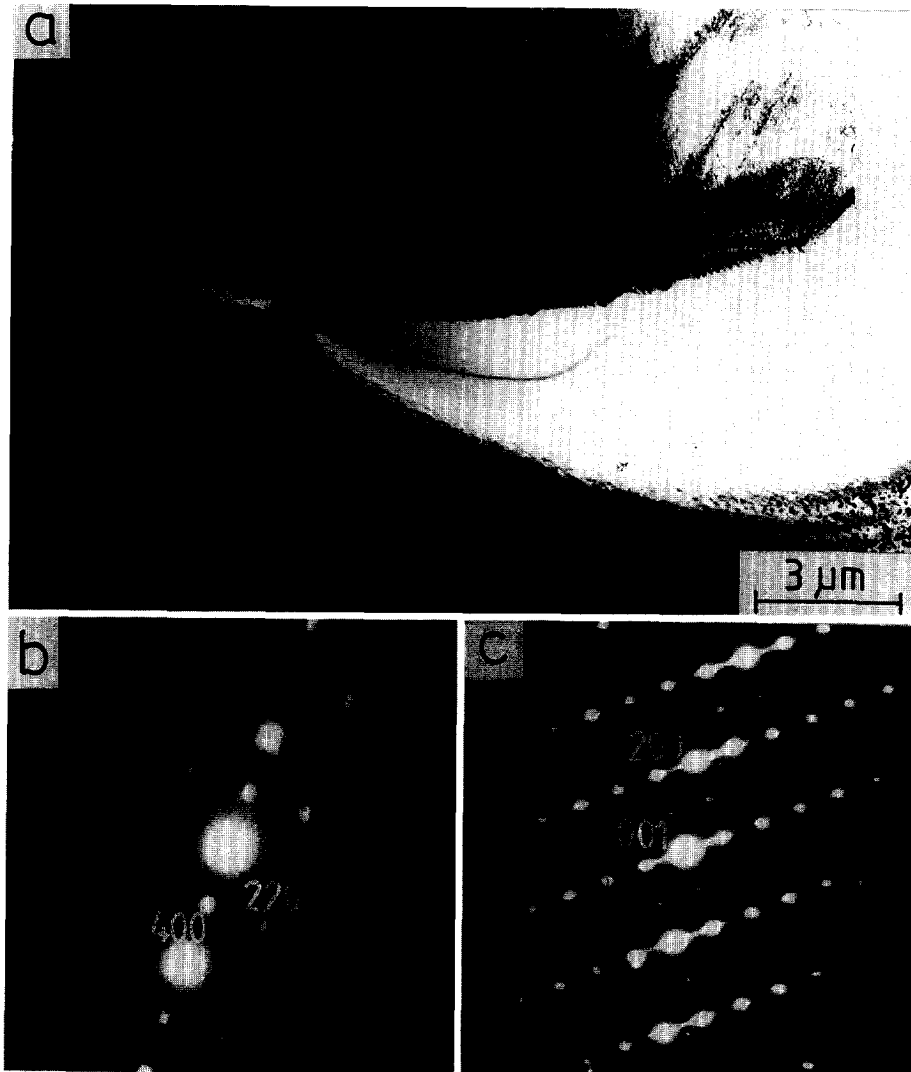curve indicate where individual micrographs (Figs 6–11) were taken.

Fig. 7. (a) Transmission electron micrograph showing propagation of 2H martensitic plate. (b) SADP taken from the matrix. (c) SADP taken from the martensite.
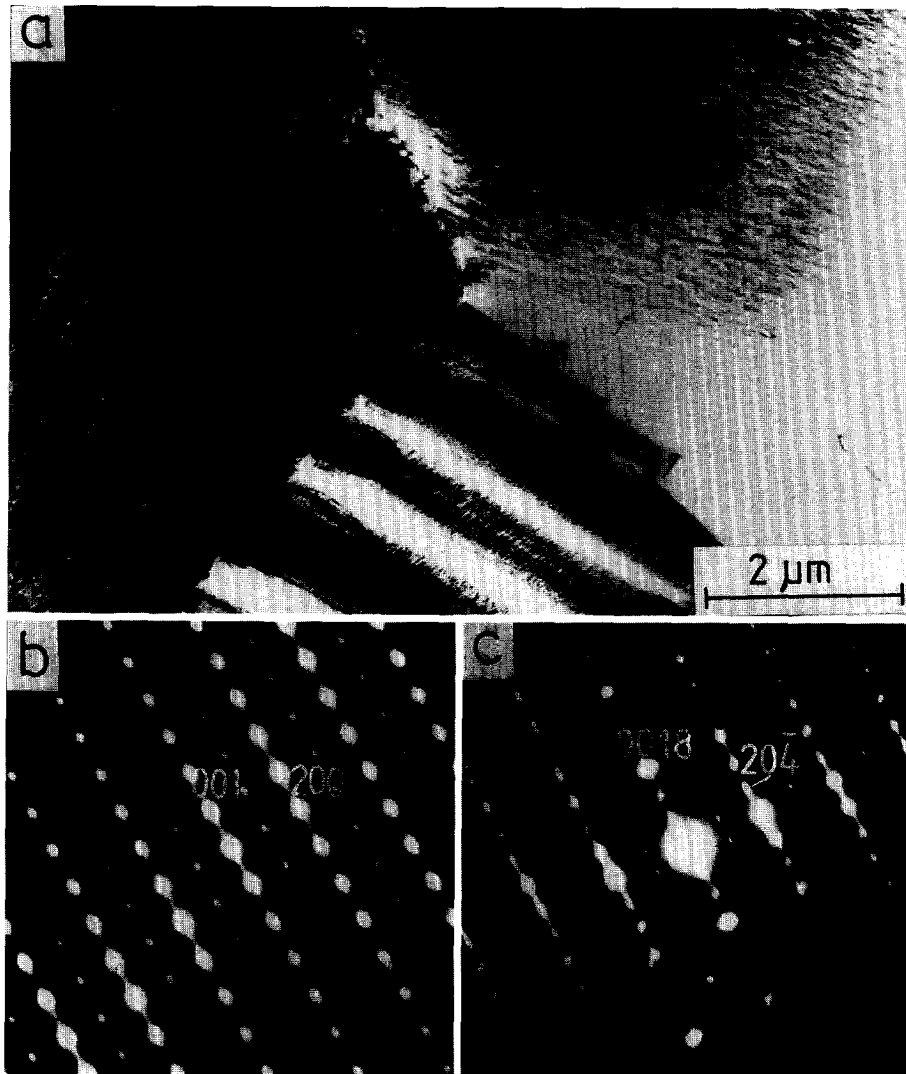
Fig. 8. (a) Transmission electron micrograph showing nucleation of the 18R martensite needles at a tip of the 2H plate. (b) SADP from the plate on the left side of the micrograph. (c) SADP from the needles formed on the right side of the plate.

Fig. 9. (a) Transmission electron micrograph showing propagation β_1' martensitic needles. SADP is inserted in the corner.
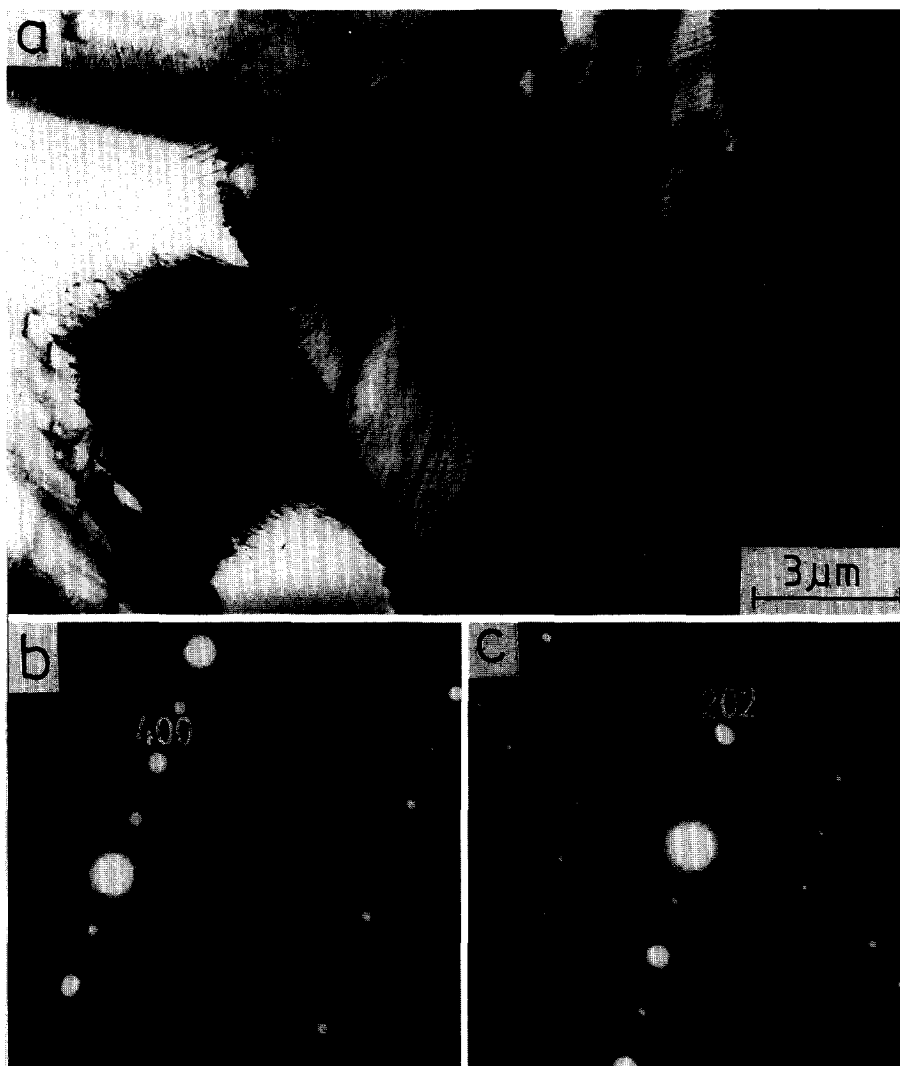

Fig. 10. (a) Transmission electron microstructure showing a dislocation structure at a relatively high degree of superelastic deformation in the $\langle 100 \rangle \beta_1$ direction. (b) SADP from the matrix on the left side of the micrograph. (c) SADP from the martensitic plate in the right side.
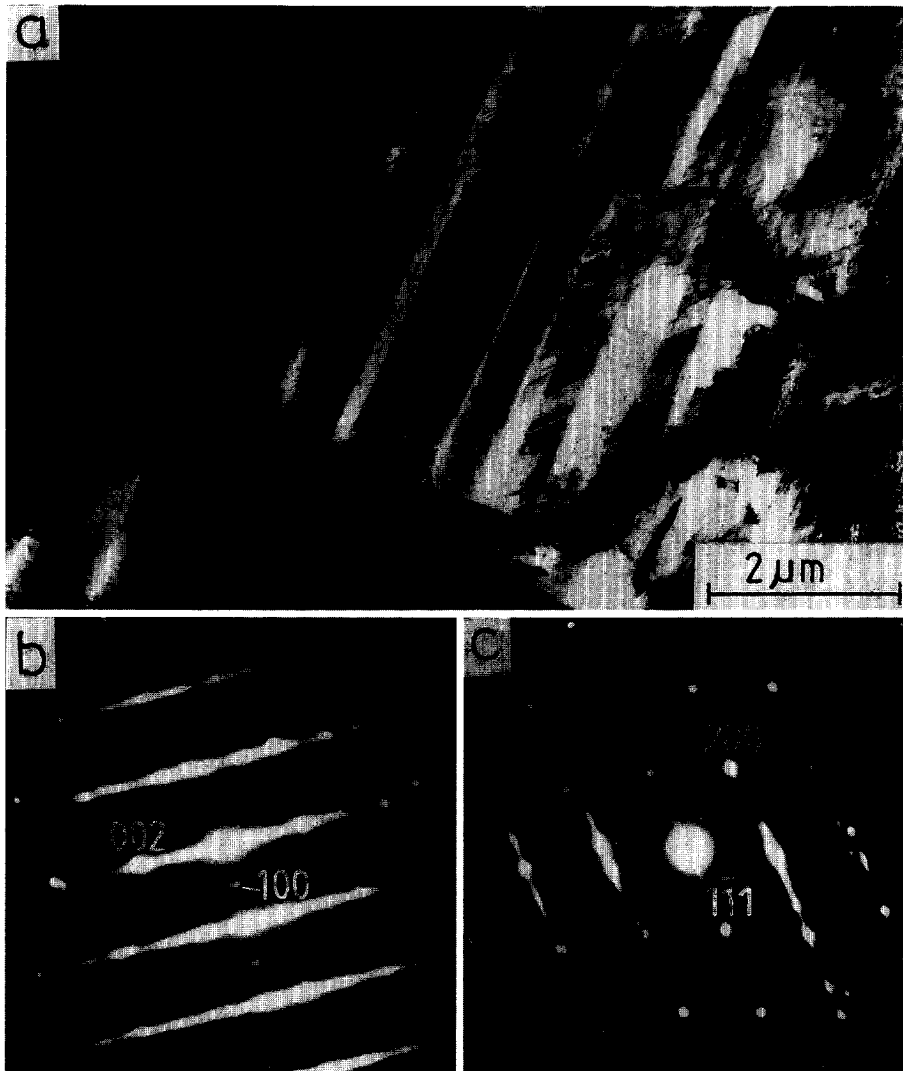
Fig. 11. (a) Tranmission electron micrograph taken after unloading, showing residual martensite of extremely high random stacking fault density. (b) SADP from the plate in the bottom of the micrograph. (c) SADP from the upper needles.

and $[1\bar{1}0]\beta_1 \| [001]\gamma_1'$. The traces of individual needles (of the same orientation) lie often along $[100]\beta_1$, i.e. parallel to the tensile direction.

The next micrograph (Fig. 8) taken at the same deformation stage shows the nucleation of individual needles of β_1' martensite at the tip of a γ_1' plate. The SADPs taken from a large and a small plate [Figs 8(b) and (c)] reveal that they possess the same crystallographic orientation (i.e. [010] zone axis parallel to the optical axis of the microscope), but different structures, i.e. 2H for the large plate and 18R for the small one. The next following image (Fig. 9) shows the propagation of the 18R martensite in the form of a stack of individual needles, as it was similarly observed in CuAlFe [15] alloys. This confirms the earlier optical microscopy observation concerning a different morphology of 2H and 18R martensites (Figs 3 and 4). Those needles grow in the $[130]\beta_1$ direction with stacking fault planes inclined by 45°

with respect to the tensile axis. The orientation relation between the 18R martensite and the parent phase is the same as that in the case of 2H. At the highest deformation applied (Fig. 10) one can see dislocations within 2H martensite in the form of pile-ups of short lines parallel to $\langle 101 \rangle \gamma_1'$. They are most probably connected with the nucleation of new variants of plate orientations due to martensite deformation. Similar dislocation structures connected with the nucleation of martensite were observed by Kikuchi and Kajiwara [21] in FeNiMo alloy. During *in situ* tensile experiments on CuAlZn alloys Gotthardt and Stoiber [22] found the nucleation and growth of martensitic needles at another plate interface by moving partial dislocations limiting stacking faults. There may be a similar situation in the case presented in Fig. 10. However, some influence of glide cannot be excluded since the dislocations do not pile up along straight lines.
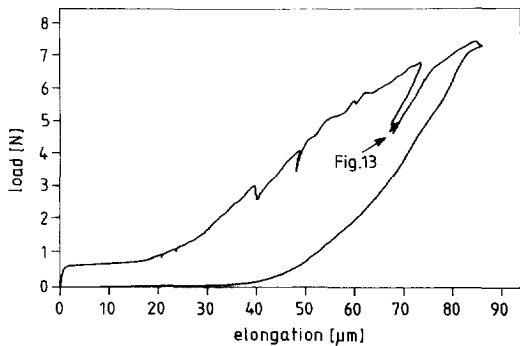
Fig. 12. Load/elongation curve obtained during *in situ* deformation from CuAlMn single crystal in the [110] direction at (001) foil orientation.

Considering the nonuniform shape of the specimen after electropolishing, a stress concentration in thin regions cannot be avoided and one may expect a plastic deformation of the martensite, causing irreversible deformation. Indeed, after unloading a significant fraction of martensite (particularly in thin regions) does not transform back to the parent phase. Figure 11 shows a micrograph taken after unloading (see Fig. 6). A SADP taken from the region of the plate in the bottom [Fig. 11(b)] shows diffuse streaks of a very high intensity owing to a correspondingly high density of random stacking faults. Barely distinguishable spots from the upper needles [Fig. 11(c)] may be indexed according to 3R and 18R crystal structures. SADP from a region visible in the lower part of the micrograph was indexed according to [010] 2H zone axis orientation,

however, one cannot exclude the presence of spots from the 18R martensite hidden within high-intensity streaks due to an extremely high density of random stacking faults. A similar observation of a very high random stacking fault density within 2H and 9R martensite layers was reported in CuZnSi alloys [23], directly quenched to martensite. This type of martensite was irreversible during heating above A_1, similarly to this in Fig. 11.

Figure 12 shows another load/elongation curve of an *in situ* tensile experiment on a single crystal in the (001)[110] orientation. There is a clear difference between this curve and the previous one [Fig. 6(a)]. The stress plateau has not been attained, even after a relatively large strain and the strain was only poorly recovered after unloading. In the electron micrograph taken at a relatively high strain (Fig. 13) one can see a martensitic plate of irregular shape and of 2H structure as determined from the SADP (inserted in Fig. 13). It shows two systems of perpendicular stacking faults indicating a twin orientation of two martensitic variants. They are separated by interface dislocations, similar to the case of Fig. 10. In the majority of plates observed for 2H or 18R structure stacking faults lie parallel to the tensile direction $\langle 110 \rangle$, i.e. they are not in a favorable orientation for a shear-type transformation. The martensite is then subjected to a plastic deformation causing its irreversibility. Finally, a poor strain recovery is observed. Tensile experiments in the $\langle 110 \rangle$ direction of bulk CuAlFe single crystals indicated a much higher yield stress to form β_1' martensite than in $\langle 100 \rangle$ directions [14]. The higher sensitivity to the tensile direction is

Fig. 13. Transmission electron microstructure taken during *in situ* pseudoelastic deformation in the $\langle 110 \rangle$ direction of the foil in the [001] zone axis orientation. SADP from the martensite is inserted in the corner of the micrograph.
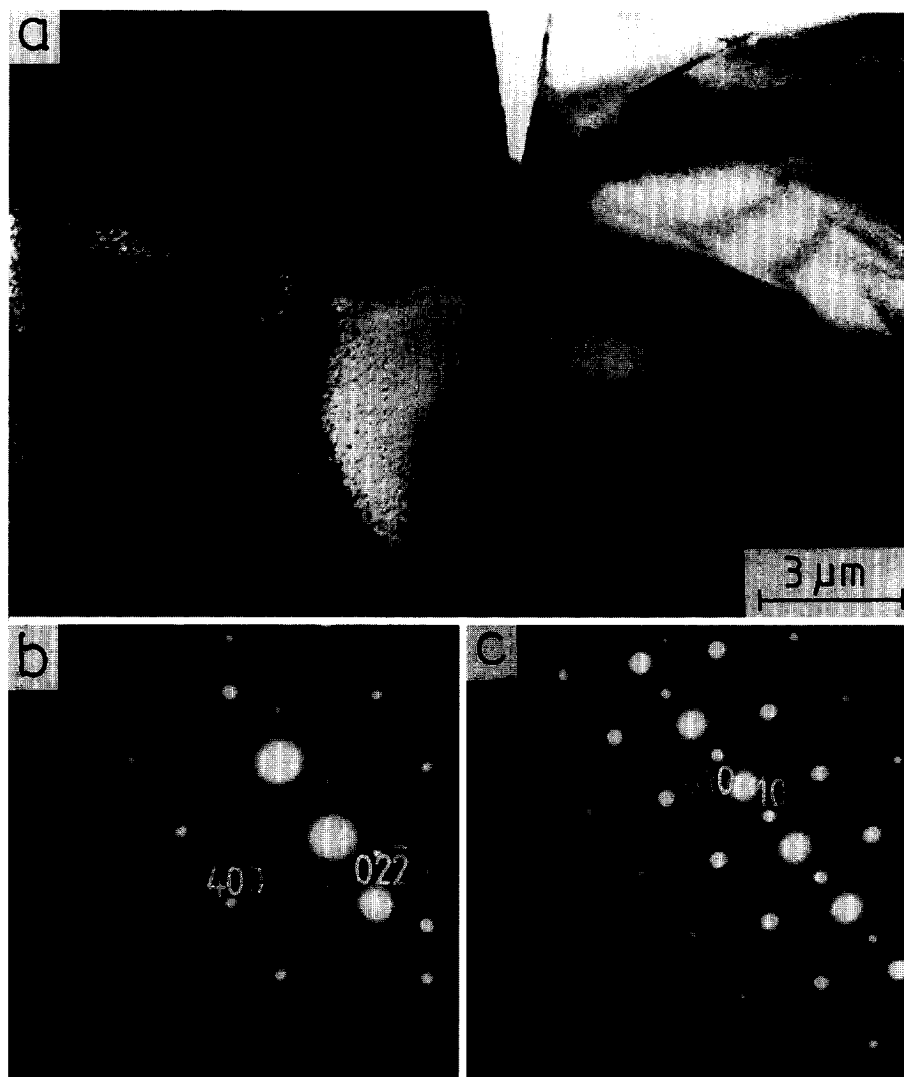
Fig. 14. (a) Transmission electron micrograph taken during *in situ* pseudoelastic deformation in the $[01\bar{1}]\beta_1$ direction at the [011] zone axis orientation. (b) SADP from the matrix. (c) SADP from the martensitic plate near the crack.

explained by other authors by a higher stacking fault energy of investigated alloys with respect to CuAlNi. The present experiments on bulk and microtensile samples clearly demonstrate a different character of
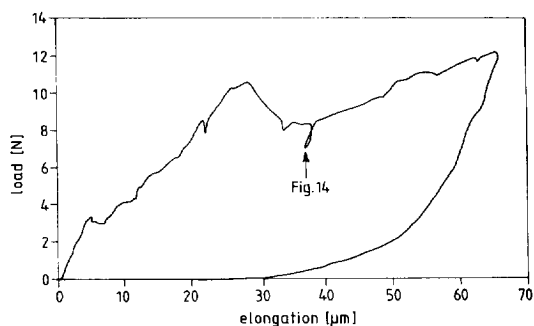

Fig. 15. Load/elongation curve taken during *in situ* pseudoelastic deformation of the sample in the $[01\bar{1}]\beta_1$ direction at the [011] foil orientation.

stress/strain curves for $\langle 100 \rangle$, $\langle 110 \rangle$ and irrational tensile directions. The explanation of Martynov *et al.* [14] is valid also in this case, however, other factors such as ordering should also be considered. Similar observations were performed on single crystals of the $(011)[01\bar{1}]$ orientation. Figure 14 demonstrates the growth of a martensitic plate near a crack at the edge of a foil. An identical crystallographic relationship like that in the case of $(001)\beta_1$ was observed, i.e. $[001]\gamma_1'\|[011]\beta_1$ and $[010]\gamma_1'\|[100]\beta_1$. The load/ elongation curve of Fig. 15 indicates that the strain only partially recovers, indicating a high sensitivity of specimens deformed in the $\langle 110 \rangle$ direction to plastic deformation. However, owing to an inhomogeneity of stress distribution in the *in situ* tensile specimens, they are subjected to an inhomogeneous deformation so that a comparison of the tensile curves to those of bulk specimens may not be appropriate. Such differences were already reported in earlier *in situ* work on CuAlFe alloys [15].

CONCLUSIONS

(1) Tensile deformation of a CuAlMn single crystal with an irrational orientation causes the formation of parallel plates at the yield stress. With increasing strain new plates are formed in front of previous ones.

(2) A stress/temperature metastable phase diagram was established for martensitic phases. With respect to the $\beta_1 \rightarrow \gamma_1'$ transformation the transformation $\beta_1 \rightarrow \beta_1'$ occurs at lower temperatures and higher stresses. However, the differences are not very large. The established diagram is different from that reported for a CuAlMn alloy of lower Mn and higher Al contents, tested in tension in a $\langle 100 \rangle$ direction.

(3) *In situ* HVEM tensile deformation of crystals at the (001)[100] orientation allowed to identify the formation of γ_1' martensite at the first deformation stages, usually in the form of single plates nucleating on the pre-existing ones. At higher strains 18R martensite is formed in stacks of very narrow needles. The following crystallographic relationship was found: $[001]\beta_1 \| [010]\gamma_1'$, β_1' and $[110]\beta_1 \| [001]\gamma_1'$, β_1'.

(4) Contrary to bulk specimens, the strain did not recover completely, even at small strains less than 2%. This was most probably due to a permanent deformation of the martensite resulting from the nonuniform stress distribution in electrolytically thinned specimen. The stabilized martensite observed after unloading possesses a very high density of random stacking faults and mixed layered γ_1', β_1' and α_1' structures.

(5) At *in situ* deformation in the $\langle 110 \rangle$ direction and $\{001\}$ or $\{110\}\beta_1$ foil orientations a much larger permanent deformation was observed after stress release. It was accompanied by an increased dislocation density inside the martensitic plates and at interfaces.

REFERENCES

1. K. Otsuka and K. Shimizu, *Int. Metals Rev.* **31**, 93 (1986).
2. Q. Jiang and H. Xu, *Acta metall. mater.* **40**, 607 (1992).
3. C. Rodriguez and L. C. Brown, *Shape Memory Effects in Alloys* (edited by J. Perkins), p. 29. Plenum Press, New York (1975).
4. N. Ono, *Met. Trans. JIM.* **31**, 855 (1990).
5. K. Shimizu and K. Otsuka, *Met. Trans. JIM* **31**, 59 (1990).
6. J. D. Eisenwasser and L. C. Brown, *Met. Trans.* **3**, 1359 (1972).
7. N. Ono, *Met. Trans. JIM.* **31**, 381 (1990).
8. T. Saburi, Y. Inada, S. Nenno and N. Hori, *J. Physique* **C4, 43**, 633 (1982).
9. J. E. Bidaux and M. Ahlers, *Z. Metallkd.* **83**, 5 (1992).
10. J. Stoiber and R. Gotthardt, *The Martensitic Transformation in Science and Technology* (edited by E. Hornbogen and N. Jost), p. 27. DGM Informationsgesselschaft Verlag, Germany (1989).
11. L. Delaey, F. Van de Voorde and R. V. Krishnan, *Shape Memory Effects in Alloys* (edited by J. Perkins), p. 351. Plenum Press, New York (1975).
12. S. Miura, Y. Morita and N. Nakanishi, *Shape Memory Effects in Alloys* (edited by J. Perkins), p. 389. Plenum Press, New York (1975).
13. H. Kato, J. Dutkiewicz and S. Miura, *Acta metall. mater.* **42**, 1359 (1994).
14. V. V. Martynov, K. Enami, A. V. Tkachenko and L. G. Khandros, *Dokl. Akad. Nauk SSSR* **258**, 608 (1981).
15. J. Dutkiewicz, V. V. Martynov and U. Messerschmidt, *J. Materials Sci.* **24**, 3904 (1989).
16. U. Messerschmidt and F. Appel, *Ultrasmicroscopy* **1**, 223 (1976).
17. R. Rapacioli, M. Chandrasekaran, M. Ahlers and L. Delaey, *Shape Memory Effects in Alloys* (edited by J. Perkins), p. 385. Plenum Press, New York (1975).
18. S. Miura, Y. Morita and N. Nakanishi, *Shape Memory Effects in Alloys* (edited by J. Perkins), p. 389. Plenum Press, New York (1975).
19. I. M. Robertson and C. M. Wayman, *Met. Trans.* **15A**, 269 (1984).
20. G. Van Tendeloo, M. Chandrasekaran and F. C. Lovey, *Met. Trans.* **17A**, 2153 (1986).
21. T. Kikuchi and S. Kajiwara, *Proceedings ICOMAT 86* (edited by Japan Institute of Metals), p. 192. Sendai (1987).
22. R. Gotthardt and J. Stoiber, *The Martensitic Transformation in Science and Technology* (edited by E. Hornbogen and E. Jost), p. 27. DGM Verlag, Oberursel (1989).
23. J. Dutkiewicz and G. Kostorz, *Phys. stat. sol. (a)* **123**, 63 (1991).